




Micro-PIXE and micro-IBIL characterization of lapis lazuli samples from Myanmar mines and implications for provenance study

Laura Guidorzi^{1,2}, Alessandro Re^{1,2,a} , Marta Magalini^{1,2}, Debora Angelici², Alessandro Borghi³, Gloria Vaggelli⁴, Fulvio Fantino⁵, Valentino Rigato⁶, Leonardo La Torre⁶, Quentin Lemasson^{7,8}, Claire Pacheco^{7,8}, Laurent Pichon^{7,8}, Brice Moignard^{7,8}, Alessandro Lo Giudice^{1,2}

¹ INFN Sezione di Torino, Via Pietro Giuria 1, Torino, Italy

² Dipartimento di Fisica, Università di Torino, Via Pietro Giuria 1, Torino, Italy

³ Dipartimento di Scienze della Terra, Università di Torino, Via Valperga Caluso, 35, Torino, Italy

⁴ CNR - Istituto di Geoscienze e Georisorse, Via Valperga Caluso, 35, Torino, Italy

⁵ Turin Thermoluminescence Analysis, Via Felice Cavallotti 33, Cuneo, Italy

⁶ INFN Laboratori Nazionali di Legnaro, Viale dell'Università 2, Legnaro, Padova, Italy

⁷ Centre de Recherche et de Restauration des Musées de France, C2RMF, 14 quai François Mitterrand, Paris, France

⁸ Fédération de Recherche FR3506 New AGLAE, 14 quai François Mitterrand, Paris, France

Received: 2 November 2022 / Accepted: 1 February 2023

© The Author(s) 2023

Abstract The provenance of raw lapis lazuli used since the Neolithic Age for the realization of carved artefacts can be pivoting for the reconstruction of ancient trade routes. The role of main provider of this material in ancient times is generally attributed to the Badakhshan quarries (Afghanistan), although other deposits could have been exploited as well since antiquity. The systematic multi-technique analysis of lapis lazuli rocks coming from four known source areas (located in present-day Afghanistan, Tajikistan, Siberia and Chile) has led in the last years to the compilation of a protocol for provenance determination. The protocol is based on differences in the physical–chemical properties measured with non-invasive techniques (Ion Beam Analysis (IBA)), making it suitable also for precious ancient artefacts. In this work, 10 new reference samples from the Mogok quarry (Myanmar), previously subjected to a complete petrographic and mineralogical characterization, have been analysed employing μ -PIXE (Proton Induced X-ray Emission) and μ -IBIL (Ion Beam Induced Luminescence) techniques. The subdivision of Myanmar samples into three groups, previously suggested, is corroborated by diopside trace elements concentrations. The results also allow to include Myanmar as a new provenance in the analytical protocol, indicating that provenance markers such as presence/absence of wollastonite, altered pyrites and Sr content are still valid to discriminate also the Myanmar lapis lazuli from Chilean or Siberian ones. New weaker markers (Zn content in diopside, Se and Cu contents in pyrite) are proposed for the discrimination of Myanmar from Afghan or Tajik provenances; however, from the analysis it arose the need of investigating new mineral phases with IBA to find strong markers for a definitive discrimination with samples from Southwest Asia.

1 Introduction

Lapis lazuli is commonly classified as a metamorphic rock [1], although the mechanisms that lead to its formation are quite complex and up to now not completely understood. It is, however, certain that its generation requires precise geological conditions, occurring only in few places around the globe [2]. The Badakhshan region in Afghanistan presents the richest and most famous lapis lazuli quarries, but some other less exploited sources exist in the world, for example in Pamir Mountains (Tajikistan), near Irkutsk in the Lake Baikal area (Siberia, Russia), in the Coquimbo region (Chile), near Mogok (Myanmar) [3]. Lapis lazuli is a complex rock composed by a high number of mineral phases. The blue colour is provided by the lazurite phase ((Na, Ca)_{7.5-8} (Si, Al)₁₂ (O, S)₂₄ (SO₄, Cl)_{1.3-2}), a member of the sodalite group where sulphur ions are enclosed in cage-like structures [4]. Other main phases are diopside (CaMgSi₂O₆), calcite (CaCO₃), wollastonite (CaSiO₃) and pyrite (FeS). In gemmology, lapis lazuli is defined as a semi-precious stone and its value is enhanced by its peculiar colour and rarity. In fact, it has been appreciated and used since the VII millennium BCE and can be found in glyptic art and inlays coming from ancient sites of different civilizations, such as Ancient Egypt and the Indus Valley Civilisation [5–8]. The interest of archaeologists in this stone resides particularly on the fact that such artefacts were found at a distance of thousands of kilometres from the known lapis lazuli quarries, posing a lot of questions on the ancient trade routes connecting the sites and on the economic and social structure in ancient societies. The possibility to associate the raw material to the place of geological origin by means of scientific analysis seems to be the optimal way to provide some

^a e-mail: alessandro.re@unito.it (corresponding author)

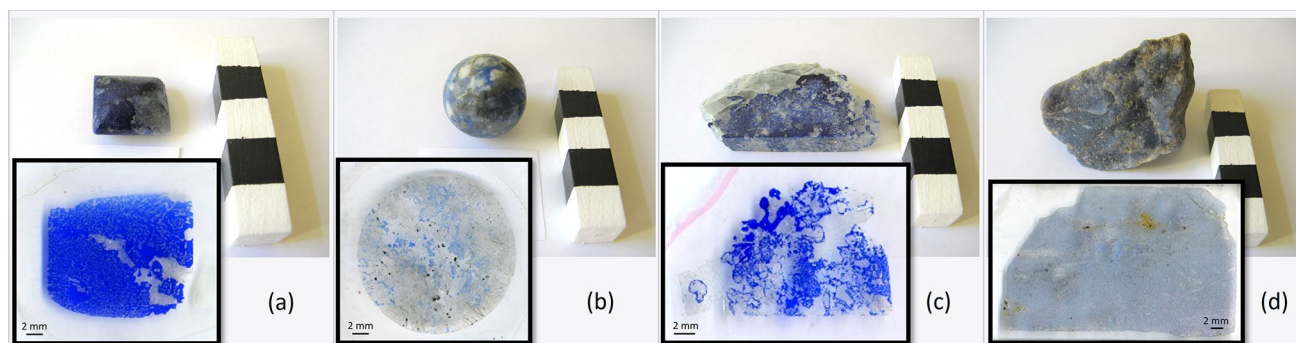


Fig. 1 A representative set of the ten lapis lazuli rock samples from Myanmar and of the corresponding thick sections: **a** MYA07 (group 1); **b** MYA10 (group 2); **c** MYA02 (group 3); and **d** MYA12. B/W scale bar = 1 cm

answers about the issue. In the past decades, several attempts at provenance studies have been performed with various purposes and methods, displaying, however, two main flaws: a limited number of samples to build a reference database [9] or the use of invasive or destructive techniques, such as Isotope Mass Spectroscopy [10] or Powder X-ray Diffraction [1], that in the case of artistic or archaeological artefacts are to be avoided as much as possible. With the aim to overcome these issues, a decade-long interdisciplinary study favouring non-invasive techniques and based on a reference set of 45 lapis lazuli rocks with certain origin was started at the Physics department of the University of Torino and is still ongoing. The analyses led to the compilation of an analytical protocol that allows to discriminate among 4 provenances (Afghanistan, Tajikistan, Siberia and Chile) using provenance markers identified with microscopy and Ion Beam Analysis (IBA) techniques [11]. In particular, Chilean lapis lazuli is of easy identification, due to the widespread presence of wollastonite [12–15]. Siberian samples, instead, are the only ones characterized by iron oxide-hydroxide minerals pseudomorphosed after pyrite [16, 17]. These samples also present a Sr content higher than about 180 ppm in diopside crystals [15, 17]. In samples from Tajikistan and Afghanistan, well-preserved and idiomorphic pyrite crystals are generally detected and these two provenances can be discriminated on the basis of the trace element content in this mineral phase [17]. These kind of features, that are present in all samples from a given provenance, are considered strong markers. Regarding instead the “weaker” markers, present only in some of the analysed rocks, diopside crystals in Afghan samples show a Ti content above 710 ppm, V content above 210 ppm and Cr content above 220 ppm, together with a strong ionoluminescence band centred at about 770 nm [15]. Recently, new samples from Myanmar were acquired and a previous petrographic and minerochemical study has been undertaken by means of SEM-EDX for the geochemical characterization of both major and minor mineral phases [18]. These samples have been now analysed with μ -PIXE (Particle Induced X-rays Emission) and μ -IBIL (Ion Beam Induced Luminescence) in search for new markers that could allow the extension of the provenance protocol.

2 Samples

The ten lapis lazuli samples were acquired in Myanmar: they are not georeferenced, but they came with a provenance certification from Mogok (Mandalay region), where different extraction mines are present [19]. They were prepared as thick petrographic sections (about 100 μ m thickness) and carbon-coated before Ion Beam Analysis to avoid charging effects during the measurements in vacuum. Representative images of the whole rocks and of the obtained sections can be seen in Fig. 1. According to the characterization with optical and electron microscopy (BSE: Back-Scattered Electrons) and with SEM-EDX (Scanning Electron Microscope – Energy-Dispersive X-ray spectroscopy) reported in a previous work [18], the main paragenesis is constituted by diopside, lazurite and calcite with apatite and pyrite as accessory minerals. The samples can also be divided into three main groups on the basis of the identified mineral phases: (1) the diopside–calcite group, with samples MYA07, MYA08 and MYA09; sample MYA12 is also tentatively placed in this group, despite showing important differences with respect to other samples, as described in [18]; (2) the nepheline–hauyne group, with samples MYA10 and MYA11; and (3) the amphibole group, with samples MYA02, MYA03, MYA04 and MYA06.

3 Instruments and analytical methods

The Ion Beam Analysis was focused on the mineral phases reported so far in the provenance protocol [11], namely wollastonite, diopside and pyrite. Target crystals were identified in the thick sections via preliminary characterization with optical microscopy, cold-cathodoluminescence (cold-CL) and electron microscopy: all the instrumentation is hosted at the Earth Science Department of the University of Torino [18, 20]. As an example, an area of sample MYA07 is shown in Fig. 2: different minerals, identified by means of BSE images and SEM-EDX microanalysis, show different luminescence features with cold-CL. In general, the luminescence

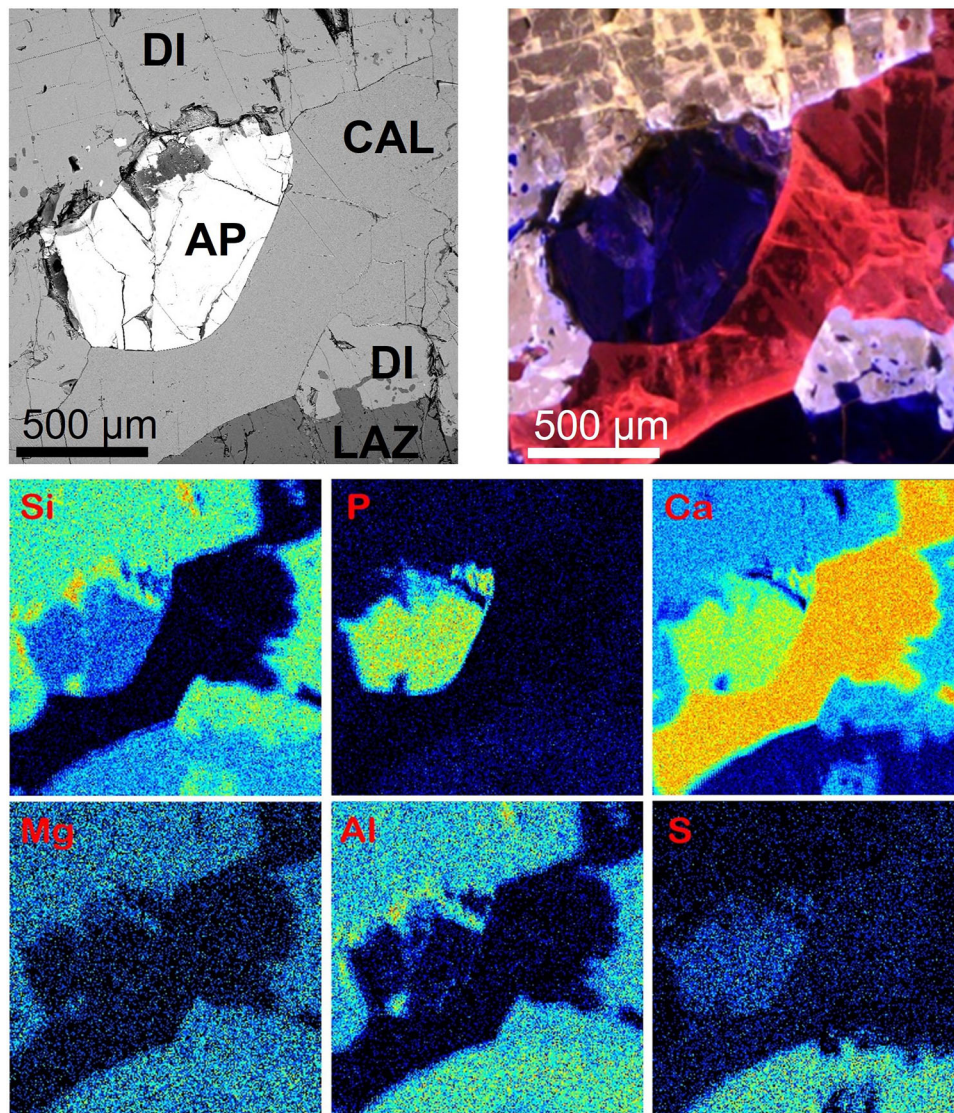


Fig. 2 Representative SEM-BSE (top left) and cold-CL (top right) images and μ -PIXE maps acquired at INFN-LNL (bottom) for sample MYA07. In μ -PIXE maps an area larger than for other analyses is reported. AP = apatite; CAL = calcite; DI = diopside; and LAZ = lazurite

colour is yellowish-white in diopside, red-orange in calcite and dark-blue in lazurite, whereas pyrite is not luminescent [14]. Target crystals were chosen among the biggest in size (at least $100\ \mu\text{m}$ in diameter) to ensure that the ion probed volume is fully included inside them. Finally, during Ion Beam Analysis, μ -PIXE maps were used to select the final area of analysis. As for lapis lazuli from other provenances, diopside crystals in Myanmar samples show a zonation phenomenon, observable in cold-CL images as differences in the luminescence intensity, due in part to different amounts of trace elements. To take into account this variability, it is necessary to select and analyse many areas in a sample. In particular, in this work a total of 43 areas, ranging from 3 to 5 for each sample, were selected in diopside crystals. For pyrite, instead, only 8 areas were suitable for IBA, due to the small crystal dimensions, and they were specifically limited to samples MYA07 (group 1), MYA10 and MYA11 (group 2), MYA02 and MYA06 (group 3) and MYA12. During the selection, particular attention was paid in considering only crystals that showed a S/Fe content ratio typical of pyrite (1.1 ± 0.2) to avoid other iron sulphide minerals as, for example, pyrrhotite (Fe_{1-x}S ($x=0-0.17$)).

IBA measurements in vacuum (ca. 10^{-5} mbar) were carried out at the AN2000 accelerator of INFN-LNL laboratories (Legnaro, Padova, Italy), specifically dedicated to interdisciplinary research based on ion beams [11, 21–23], with a 2 MeV protons microbeam (beam size ca. $6\ \mu\text{m}$). μ -PIXE and μ -IBIL signals were acquired simultaneously for luminescent phases. For each acquisition, an area of $30 \times 30\ \mu\text{m}^2$ was scanned. The charge was measured directly on the sample holder and integrated by a pico-ammeter. The PIXE detector was a high-purity germanium (HPGe) Ortec IGLET-X, positioned at 45° with respect to the ion beam. To simultaneously analyse light and heavy elements with the same detector, an aluminium funny filter [24] was placed in front of the detector window. Spectra analysis was carried out through GUPIXWIN software (version 2.2.3) [25] using a set of reference mineral standards (SPI

Table 1 Summary and comparison of the specifics for the ion beam analysis facilities used for lapis lazuli analysis in this work: general features and μ -PIXE and μ -IBIL experimental conditions are listed.

		FACILITIES	
		INFN-LNL	NewAGLAE
General features	Location	Legnaro (PD), Italy	Paris, France
	Measurement type	in vacuum	in air
	Beam energy	2 MeV	3 MeV
	Beam size	5–6 μm	30–40 μm
	Average beam current	200 pA	500 pA
μ -PIXE	Detector	1 HPGe	4 SDD (1 LE and 3 HE)
	Absorbers	Al funny filter	Mylar (100 μm) for HE
	Acquisition software	OM-DAQ	AGLAE-ACQ
μ -IBIL	Collimating lens	74-UV (200–2000 nm)	–
	Optical fibre	QP600-1-UV-VIS + P600-025-UV-VIS $\varnothing=600 \mu\text{m}$	QP1000-2-SR $\varnothing=1 \text{ mm}$
	Spectrometer	Ocean Optics USB4000	Ocean Optics QE65000
	Bandwidth	350–1000 nm	200–1000 nm
	Spectral resolution	2 nm	3 nm
	Acquisition software	OO Spectra Suite	AGLAE-ACQ

#02753-AB Mineral standards) for calibration. The μ -IBIL apparatus set in the vacuum chamber of the microprobe facility was introduced in 2011 by our group [26]. The photons emission induced by ion bombardment was collected through an Ocean Optics collimating lens that gathers the signal with an angle of 45° with respect to the beam direction. A system of optical fibres leads the light emitted from the sample to the spectrometer. The instrument used in this work is an Ocean Optics USB4000 spectrometer with a 350–1000 nm bandwidth and a 2 nm spectral resolution.

Measurements with extracted beam were also performed on diopside crystals at NewAGLAE facility (C2RMF, Paris, France) with a 3 MeV protons beam, in the framework of SIBILLA project (via IPERION CH and IPERION HS, EU Transnational Access programmes). The beam spot dimension was about 40 μm , and the current set-up is well described in [27]. The μ -PIXE set-up relies on a set of four SDD detectors: one detector, placed at 45° relative to the beam axis, is dedicated to the measurement of low-energy (LE) X-rays (1–10 keV); the other three SDD detectors, screened with 100 μm Mylar absorbers and positioned with a 50° relative angle to the beam axis, are dedicated to measure high energy (HE) X-rays ($>3 \text{ keV}$), greatly increasing the statistics for the detection of trace elements. Helium is fluxed in front of the low-energy detector to improve the detection efficiency of low-energy X-rays, reducing their absorption by air components. The charge is monitored by recording Si X-rays emitted by the Si_3N_4 100 nm thick exit window by means of a dedicated SDD detector. Using the mechanical scanning mode acquisition, it is possible at this facility to combine a vertical magnetic scanning of the beam (“pen”) with a horizontal target translation for the fast acquisition of elemental maps and corresponding spectra. The pen size is selectable from 50 μm to 1 mm: in this work it was used a 250 μm pen. The IBIL set-up consists in a 1 mm diameter optical fibre placed at 45° angle with respect to the beam direction that collects the light and leads it to an Ocean Optics QE65000 spectrometer recording from 200 to 1000 nm with a resolution of 3 nm (using a 100 μm entrance slit) [28]. All the IBIL spectra were corrected in intensity for the instrumental efficiency at different wavelengths. The great advantage of this system mainly consists in the simultaneous acquisition of PIXE and IBIL 2D information (both spectra and maps), that can be handled after acquisition with the homemade software AGLAEMap [29]. The quantitative elemental analysis is performed instead via TRAUIXE [29], a custom-made software based on the aforementioned GUPIXWIN that can combine low and high energy PIXE spectra using a single element as pivot. Standards used for calibration in this facility are diorite (DrN, Service d’Analyse des Roches et des Minéraux), granite (MA-N, Group International de Travail “Etalons Analytiques des Minéraux, Minerais et Roches”) and phlogopite (Mica-Mg, Centre de Recherche Petrographiques et Geochimiques) pellets made from powder, all of them rich in numerous different elements. In Table 1, a short comparison of the two facilities is reported. Tests performed by measuring certified standards and lapis lazuli samples confirmed that the quantitative results obtained in the two facilities are comparable, within a 2 sigma error.

Table 2 Quantitative results for μ -PIXE analysis on 43 diopside crystals in reference geological samples from Myanmar. Measurements tagged with the star symbol have been acquired at NewAGLAE. Data are reported in ppm as concentration \pm error and relative limit of detection (LOD); As, Pb and Y concentrations are not reported because for all crystals they resulted below detection limit (bdl)

Sample	Group	Ti	V		Cr		Mn		Fe		Cu		Zn		Sr		Zr		
			Conc.	LOD	Conc.	LOD	Conc.	LOD	Conc.	LOD	Conc.	LOD	Conc.	LOD	Conc.	LOD	Conc.	LOD	
MYA02	3	700 \pm 100	48	270 \pm 40	48	bdl	60	77 \pm 12	13	680 \pm 100	10	bdl	10	35 \pm 6	4	bdl	34	120 \pm 30	37
		610 \pm 90	47	280 \pm 40	48	bdl	60	75 \pm 12	11	830 \pm 120	9	bdl	6	56 \pm 8	3	bdl	35	100 \pm 30	35
		330 \pm 50	45	160 \pm 30	42	bdl	53	50 \pm 11	13	630 \pm 100	7	15 \pm 5	6	41 \pm 6	7	bdl	22	70 \pm 30	34
MYA03	3	390 \pm 60	48	140 \pm 30	43	bdl	36	52 \pm 13	13	650 \pm 100	11	bdl	11	27 \pm 5	5	bdl	27	80 \pm 30	30
		380 \pm 60	48	170 \pm 30	43	bdl	40	49 \pm 12	13	650 \pm 100	11	bdl	5	25 \pm 6	7	bdl	23	bdl	37
		290 \pm 40	50	190 \pm 30	44	bdl	63	79 \pm 12	12	590 \pm 90	8	bdl	9	21 \pm 5	6	bdl	40	bdl	27
*		431 \pm 13	12	137 \pm 8	12	bdl	8	69 \pm 4	6	804 \pm 9	2	bdl	8	34 \pm 3	3	28 \pm 7	8	70 \pm 13	14
*		391 \pm 8	7	108 \pm 5	8	9 \pm 3	4	66 \pm 2	3	774 \pm 7	2	bdl	5	34 \pm 2	2	13 \pm 3	3	47 \pm 6	6
MYA04	3	bdl	46	bdl	65	32	78 \pm 14	15	1850 \pm 280	10	bdl	12	120 \pm 20	6	bdl	41	bdl	43	
		360 \pm 50	46	240 \pm 40	41	bdl	36	68 \pm 12	15	1100 \pm 160	10	bdl	6	60 \pm 9	5	bdl	22	80 \pm 30	32
		330 \pm 50	47	230 \pm 40	42	bdl	63	80 \pm 12	12	960 \pm 140	10	bdl	6	61 \pm 9	5	bdl	24	130 \pm 30	35
*		357 \pm 7	6	121 \pm 4	6	bdl	4	72 \pm 2	2	977 \pm 6	2	bdl	4	54 \pm 2	2	13 \pm 2	2	119 \pm 7	5
*		310 \pm 20	19	132 \pm 12	17	bdl	12	69 \pm 7	9	1170 \pm 20	7	bdl	16	46 \pm 5	4	bdl	13	bdl	32
MYA06	3	550 \pm 80	48	210 \pm 30	48	bdl	60	79 \pm 13	12	980 \pm 150	9	bdl	12	83 \pm 12	6	bdl	21	90 \pm 30	28
		560 \pm 80	47	160 \pm 30	45	bdl	34	80 \pm 12	11	520 \pm 80	9	13 \pm 4	6	26 \pm 6	6	bdl	31	80 \pm 30	31
		570 \pm 90	47	240 \pm 40	45	bdl	34	74 \pm 13	11	780 \pm 120	10	bdl	6	49 \pm 7	5	bdl	37	100 \pm 30	37
*		480 \pm 7	5	134 \pm 4	6	9 \pm 2	3	66 \pm 2	2	1076 \pm 8	1	bdl	2	77 \pm 1	1	10 \pm 2	1	60 \pm 4	2
*		658 \pm 7	5	156 \pm 5	8	8 \pm 2	4	67 \pm 2	2	696 \pm 4	2	bdl	2	33 \pm 1	1	12 \pm 2	1	72 \pm 5	3
MYA07	1	130 \pm 40	61	150 \pm 30	50	bdl	69	110 \pm 20	12	1400 \pm 210	10	bdl	12	100 \pm 20	7	bdl	27	bdl	44
		470 \pm 70	55	230 \pm 30	51	bdl	45	76 \pm 14	15	1460 \pm 220	11	bdl	11	100 \pm 20	6	bdl	40	100 \pm 30	39
		660 \pm 100	51	260 \pm 40	50	bdl	64	80 \pm 13	12	1430 \pm 220	11	bdl	11	100 \pm 20	5	bdl	25	100 \pm 30	38
*		518 \pm 7	5	143 \pm 4	7	8 \pm 2	4	66 \pm 2	2	1340 \pm 7	2	bdl	3	68 \pm 2	2	8 \pm 2	2	59 \pm 5	5

Table 2 continued

Sample	Group	Ti		V		Cr		Mn		Fe		Cu		Zn		Sr		Zr	
		Conc.	LOD	Conc.	LOD	Conc.	LOD	Conc.	LOD	Conc.	LOD	Conc.	LOD	Conc.	LOD	Conc.	LOD	Conc.	LOD
MYA08	1	390 ± 60	46	150 ± 30	43	bdl	36	75 ± 12	13	710 ± 110	7	9 ± 4	5	46 ± 7	6	bdl	37	100 ± 30	28
		380 ± 60	68	190 ± 40	60	bdl	72	70 ± 13	18	740 ± 110	15	bdl	7	47 ± 7	6	bdl	26	bdl	43
MYA09	1	400 ± 60	54	100 ± 30	49	bdl	63	82 ± 14	14	1260 ± 190	8	bdl	10	100 ± 20	7	bdl	41	bdl	43
		bdl	83	80 ± 30	42	bdl	39	80 ± 20	15	1870 ± 280	9	bdl	11	120 ± 20	4	bdl	33	bdl	51
		bdl	59	bdl	77	bdl	66	100 ± 20	14	2400 ± 360	10	bdl	11	140 ± 20	7	bdl	26	bdl	58
		170 ± 40	53	100 ± 30	48	bdl	39	87 ± 14	13	1360 ± 200	10	bdl	13	100 ± 20	6	bdl	28	bdl	61
*		244 ± 5	5	56 ± 3	5	bdl	3	70 ± 2	2	1487 ± 10	1	bdl	2	78 ± 2	1	15 ± 2	2	bdl	4
*		106 ± 4	5	bdl	4	bdl	2	74 ± 2	2	1953 ± 12	1	bdl	2	104 ± 2	1	12 ± 2	1	bdl	4
MYA10	2	680 ± 100	52	bdl	56	bdl	58	240 ± 40	16	4930 ± 740	14	bdl	7	34 ± 6	6	bdl	30	180 ± 40	49
		540 ± 80	54	150 ± 30	52	bdl	65	240 ± 40	13	4260 ± 640	14	bdl	13	24 ± 6	6	90 ± 20	22	220 ± 40	49
*		415 ± 6	5	32 ± 3	6	bdl	4	208 ± 3	2	3830 ± 20	3	bdl	3	20 ± 1	1	35 ± 3	2	140 ± 6	5
*		428 ± 15	13	34 ± 8	14	bdl	8	230 ± 7	6	3400 ± 22	6	bdl	6	24 ± 3	3	52 ± 9	8	140 ± 20	22
MYA11	2	550 ± 80	47	90 ± 30	47	bdl	36	260 ± 40	13	4580 ± 690	14	bdl	11	29 ± 6	6	bdl	23	120 ± 30	42
		510 ± 80	47	80 ± 30	46	bdl	35	270 ± 40	15	4550 ± 680	13	bdl	7	36 ± 6	5	70 ± 20	24	90 ± 30	45
*		452 ± 13	11	29 ± 7	12	bdl	10	225 ± 6	5	4410 ± 40	5	bdl	6	28 ± 3	3	57 ± 8	10	90 ± 20	18
*		440 ± 20	16	28 ± 9	16	bdl	14	231 ± 8	8	4190 ± 40	9	bdl	14	26 ± 4	5	180 ± 20	16	60 ± 20	36
MYA12	1?	360 ± 50	48	bdl	44	bdl	58	91 ± 14	14	1990 ± 300	11	bdl	10	bdl	4	70 ± 20	26	110 ± 30	48
		310 ± 50	46	90 ± 20	41	bdl	33	80 ± 13	12	1900 ± 290	13	bdl	9	bdl	10	bdl	27	110 ± 30	40
*		400 ± 60	46	90 ± 30	42	bdl	55	130 ± 20	12	2560 ± 380	14	bdl	9	bdl	5	bdl	22	120 ± 30	36
*		349 ± 6	5	bdl	6	bdl	3	101 ± 2	2	2242 ± 14	2	bdl	3	6 ± 1	1	26 ± 3	2	89 ± 6	6
*		310 ± 20	29	bdl	24	bdl	22	103 ± 9	10	2730 ± 30	7	bdl	17	bdl	7	160 ± 30	34	bdl	66

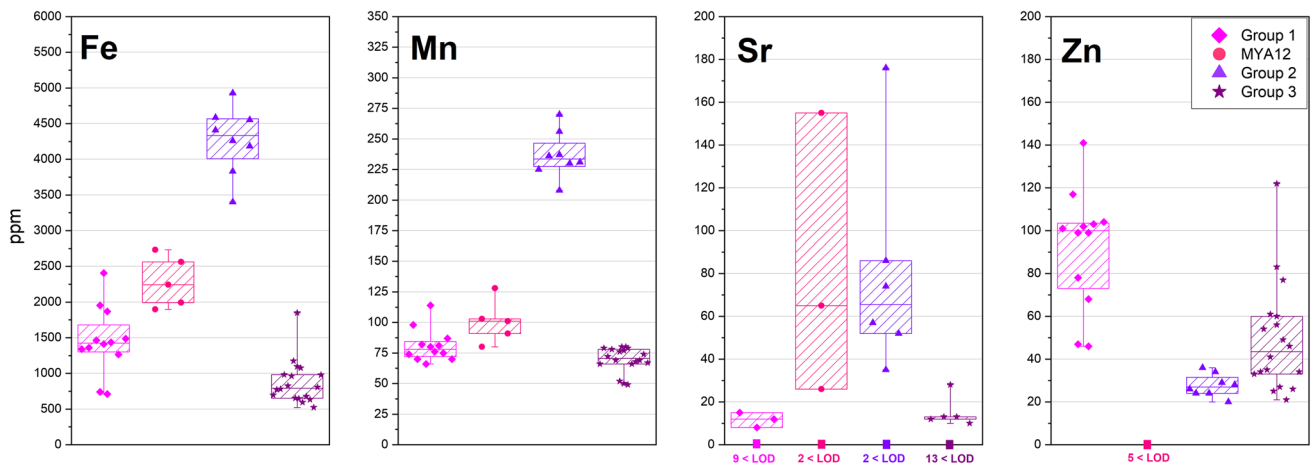


Fig. 3 Content in ppm of Fe, Mn, Sr and Zn in diopside for the three different Myanmar groups and MYA12. The box plots represent the dispersion of the experimental points: the median line and the two percentile values 0.25 and 0.75. The squared symbols in correspondence to 0 value represent the number of measurements below the limit of detection (LOD)

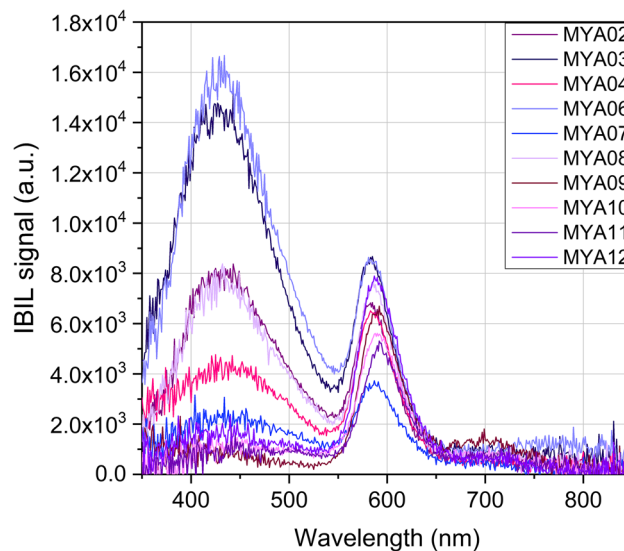


Fig. 4 Representative μ -IBIL spectra for diopside crystals measured in Myanmar samples at INFN-LNL

4 Results and discussion

An in-depth description of the mineralogical phases observed in the different rock groups can be found in [18]. About wollastonite, diopside and pyrite, the first relevant result arising from the application of IBA to Myanmar samples was obtained by means of a quick scan of the beam over the whole thick section: the strong IBIL signal characteristic of wollastonite [14] was not found, confirming the outcome of petrographic analysis [18]. Instead, it was observed an IBIL signal with a main band centred at 585 nm that is typical of diopside [15]. The results obtained from μ -PIXE measurements on diopside crystals are reported in Table 2. Major and minor elements previously quantified in [18] are not reported, but it is interesting to observe that Fe was detected by means of SEM-EDX only in samples MYA10 and MYA11 (group 2), i.e. the samples that in μ -PIXE measurements have the higher Fe content on average. Instead, all other elements listed in Table 2 were under limit of detection (LOD) using SEM-EDX.

When separating the analysed diopside crystals according to the sample grouping previously mentioned, it can be seen an evident discrimination between group 2 and the others as regards the Mn and Fe contents (Fig. 3). For the two samples belonging to group 2, Mn is always detected above 210 ± 3 ppm, whereas Fe is over 3400 ± 20 ppm. Moreover, Sr content is lower than 36 ± 7 ppm in all the diopside crystals except in group 2 (max. 180 ± 20 ppm) and MYA12 (max. 160 ± 20 ppm) samples. However, as it is thoroughly explained in [18], sample MYA12 is a peculiar case for its paragenesis and its assignation to group 1 is tentative. A difference in MYA12 with respect to other group 1 samples is also observed in Zn content, that is very low and completely below the LOD only in this sample. This grouping could be due to the provenance of the analysed samples from different mines located in the Mogok area, and it allows to underline that for this kind of provenance studies it is important to consider many samples from an extraction

Table 3 Quantitative results for μ -PIXE analysis at INFN-LNL on 8 pyrite crystals in reference geological samples from Myanmar. Data are reported in ppm as concentration \pm error and relative limit of detection (LOD); bdl=below detection limit. In the case of MYA06 and MYA12, two pyrite crystals were analysed

Sample	Group	Ni		Cu		Zn		As		Se		Mo	
		Conc.	LOD	Conc.	LOD	Conc.	LOD	Conc.	LOD	Conc.	LOD	Conc.	LOD
MYA02	3	550 \pm 50	52	210 \pm 30	35	270 \pm 30	34	500 \pm 20	27	42 \pm 14	20	100 \pm 30	37
MYA06	3	500 \pm 50	48	bdl	34	bdl	33	bdl	36	bdl	17	bdl	56
		430 \pm 50	45	bdl	33	bdl	50	bdl	21	bdl	18	bdl	51
MYA07	1	bdl	52	bdl	38	bdl	55	bdl	24	bdl	19	bdl	66
MYA10	2	110 \pm 40	47	220 \pm 30	33	bdl	32	170 \pm 20	18	38 \pm 12	17	bdl	31
MYA11	2	bdl	84	bdl	35	bdl	35	60 \pm 20	22	52 \pm 13	13	bdl	44
MYA12	1?	260 \pm 40	39	bdl	28	bdl	41	bdl	18	540 \pm 20	14	bdl	37
		150 \pm 40	47	710 \pm 40	30	bdl	53	70 \pm 20	23	110 \pm 20	19	100 \pm 30	30

area to take also into account differences in trace elements due to the paragenesis. At the same time, such differences could be used to distinguish among extraction mines in the same area.

Diopside crystals present also a strong luminescence investigated by means of μ -IBIL. In Fig. 4, a representative set of spectra acquired for the analysed diopside crystals is shown. They present the typical main band at 585 nm attributed to the presence of Mn^{2+} ions and a much smaller band at 690 nm that could be due to V^{2+} or Fe^{3+} [30]. Only for sample MYA06, the latter band seems to spread wider on a range from 700 nm to 850 nm. Most of the samples also show the very broad band around 450 nm, attributed to the TiO_6 complex [30].

About pyrite crystals, they are well preserved, but smaller and in lower amounts compared to lapis lazuli from other provenance areas. The results from μ -PIXE measurements on pyrite crystals are reported in Table 3, where only trace elements found above the detection limit were considered. Although the number of measurements for each group is low, also in this case some differences among them can be observed. In particular, samples from group 3 seems to have a higher content in Ni than other samples. Moreover, Se and Cu contents seem to be higher in MYA12 than in all other samples. Also, the occurrence in pyrite of Se and, to a lesser degree, of As as substitutes of S may be considered as peculiar of the Myanmar provenance among the Eurasian lapis lazuli.

4.1 Revised protocol

On the basis of Ion Beam Analysis results, a revised version of the protocol that would take into account also Myanmar lapis lazuli is proposed. Moreover, on the occasion of the protocol reformulation, a revision of previous data in the database was made, re-evaluating all the elemental concentrations and removing a few points due to the presence of contaminants. Analyses on samples confirmed that lapis lazuli from Myanmar is characterized by the absence of wollastonite as main mineral phase. Instead, diopside is one of the main minerals in all the groups, as in all lapis lazuli from other Asian sources. Hence, the presence of wollastonite as main mineral phase remains a strong marker for a Chilean provenance [12–15] and can be confirmed. In the previous protocol, selenium in pyrite was also reported as weaker marker for this provenance, because it was observed in content higher than 40 ppm only in some of the Chilean samples, with a maximum around 100 ppm [11, 14]. In Myanmar samples, selenium was measured in variable quantity starting from the LOD (around 17–19 ppm) up to 540 \pm 20 ppm. Consequentially, the Se marker is not able to distinguish Chilean from Myanmar samples, so it was ultimately decided to remove it from the protocol. As observed previously in [11], the protocol can be subject to changes on the basis of new information and as measurements on samples from different lapis lazuli sources grow.

Following the protocol, Siberian samples continue to be the only ones characterized by iron oxide-hydroxide minerals pseudomorphosed after pyrite [16, 17], because in Myanmar samples pyrite crystals are well formed: this allows to confirm altered pyrites as a strong marker for the Siberian provenance. Moreover, in the previous protocol we considered as an additional strong marker the fact that in all Siberian samples Sr content is higher than about 180 ppm in diopside crystals [15, 17]. In Myanmar lapis lazuli, Sr content in diopside crystals (Table 2 and Fig. 5 for a comparison to the reference dataset published in [11]) is low and not higher than 90 \pm 20 ppm nearly in all the analysed areas (96% of the total) with two exceptions: sample MYA11 (180 \pm 20 ppm) and sample MYA12 (max. 160 \pm 20 ppm). This means that the Siberian sample with the lower Sr content is indistinguishable from the Myanmar samples that have the higher contents of Sr, on the basis of this chemical element only. In the revised protocol, we decided to change this marker into a weak marker, i.e. only Siberian samples (but not all) have Sr > 200 ppm.

In the previous version of the protocol, it was shown that Tajik and Afghan samples can be discriminated on the basis of the trace element content in pyrite, in particular Cu and Ni [17]. An arbitrary line can be drawn in the Cu vs Ni plot to maintain the ideal separation between Tajikistan and Afghanistan data, with equation $Cu = 0.6 \cdot Ni$ (see Fig. 6a). In comparison with the strong markers identified for Afghanistan and Tajikistan, despite the low statistics in Myanmar samples provided by eight points (Table 3),

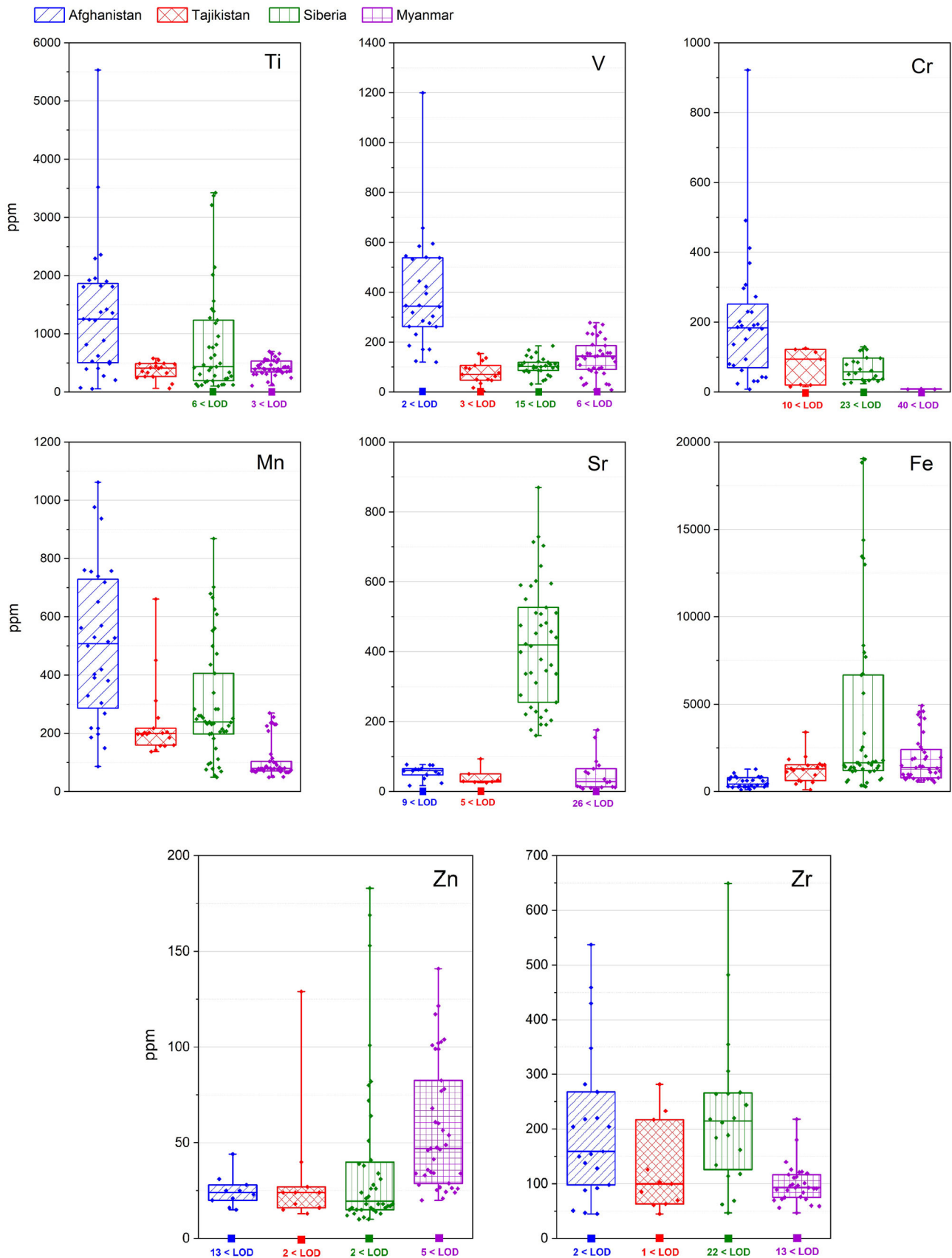


Fig. 5 μ -PIXE results for trace elements in diopside, comparing Myanmar provenance to data from the other reference geological samples [11], grouped by provenance area. The box plots represent the dispersion of the experimental points: the median line and the two percentile values 0.25 and 0.75. The squared symbols in correspondence to 0 value represent the number of measurements below the limit of detection (LOD)

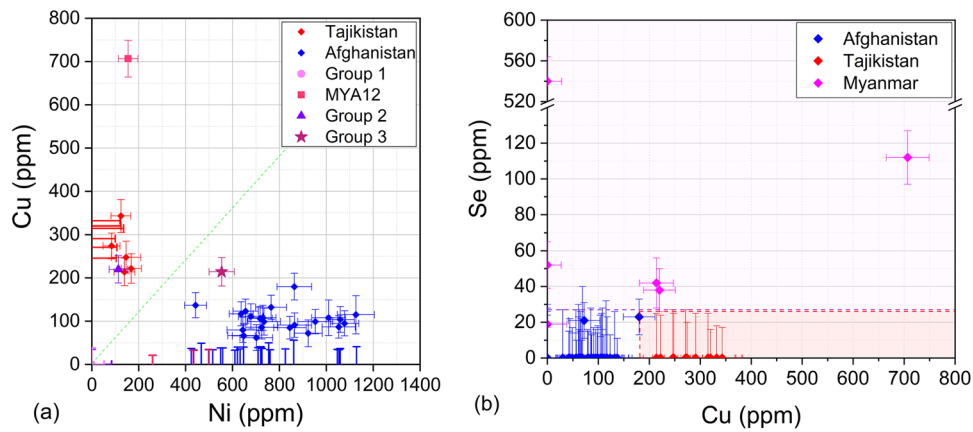


Fig. 6 Trace element contents for markers in pyrite. **a** Cu vs Ni: Myanmar samples, in purple hue, are represented with a different colour for each group defined in [18] and results are compared to data from the other reference geological samples from Southwest Asia [11]. The green dashed line defines the ideal separation between Tajikistan and Afghanistan data adopted in the new proposed protocol. **b** Se vs Cu: when evaluating only Myanmar and Tajik lapis lazuli, above a concentration of 27 ppm for Se only Myanmar samples are found (purple dashed line); the area delimited by the red dashed line contains instead only Tajik samples, defining a combination of two weaker markers

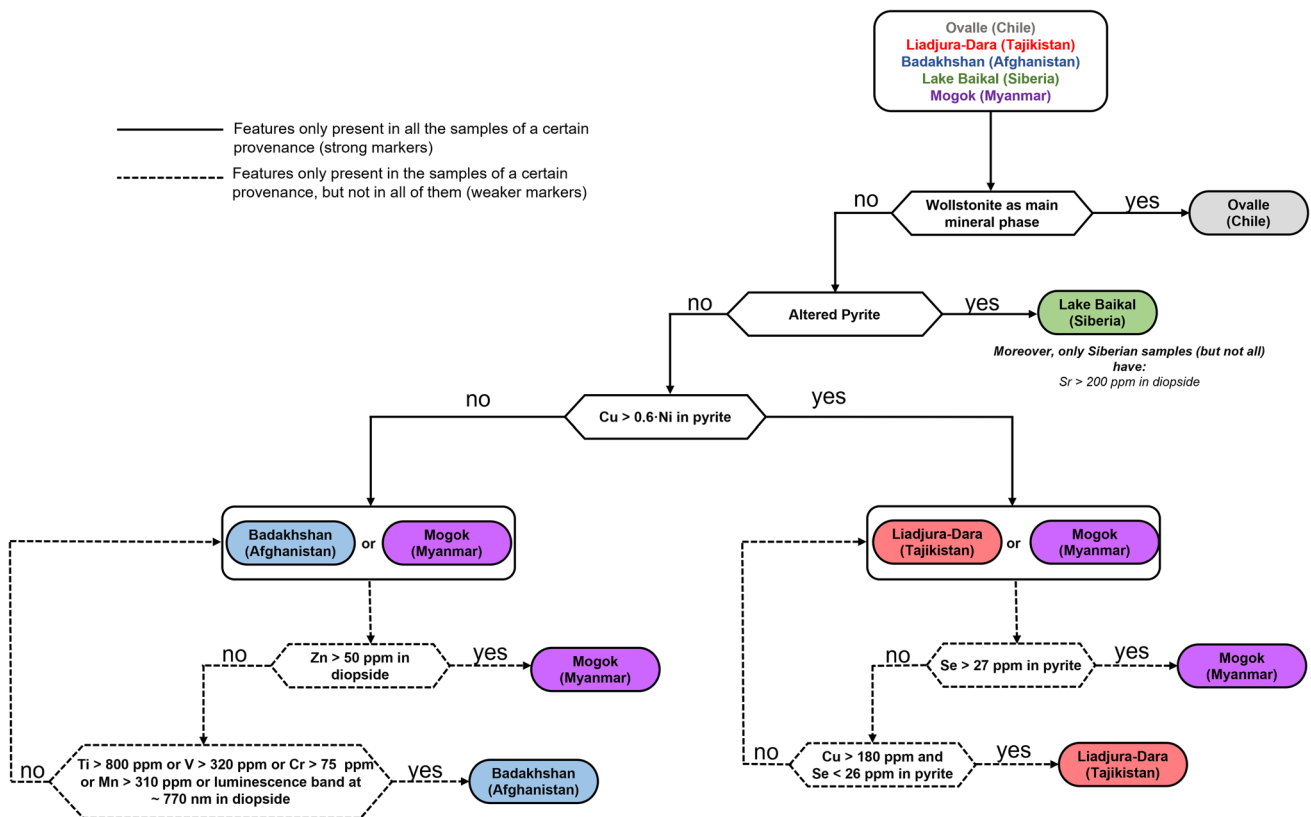


Fig. 7 The new proposed flow chart of the operative protocol, revised after taking also into account the Myanmar reference samples. Along the block chain, solid lines are used for strong markers, dashed lines for weaker markers. Additional weaker markers are reported as text next to the provenance balloon

some new considerations can be made. For all crystals, Ni content was found below 550 ± 50 ppm, whereas Cu content raised up to 710 ± 40 ppm. This certainly leads to an uncertainty in discrimination with Tajik provenance and with a fraction of the measured Afghan samples. However, if the Se content is plotted in function of Cu content (Fig. 6b), it can be noticed, first of all, that a Se concentration above 40 ppm is only characteristic of Myanmar samples, but in an uncertainty between only Myanmar and Tajik lapis lazuli this limit can be lowered to 27 ppm. Also, in the same binary comparison, a combination of the two conditions Cu content above 180 ppm and Se content under 26 ppm identifies an area where only Tajik samples are present. Nevertheless, the discrimination of Myanmar samples with Tajik or Afghan ones can rely so far only on weaker markers.

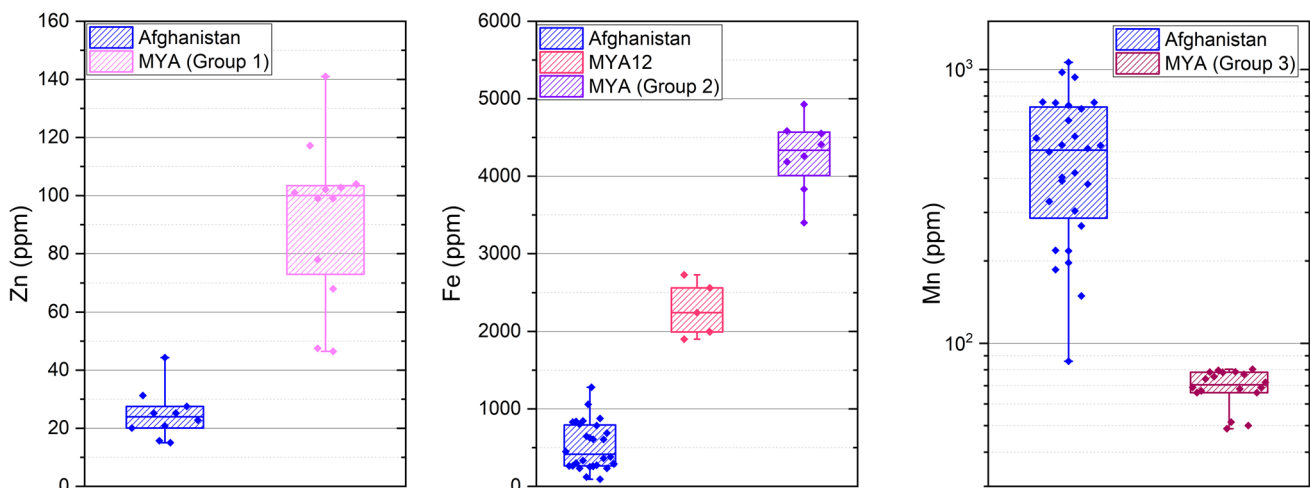


Fig. 8 Comparison between the content of Zn, Fe and Mn in diopside for Afghan samples (database) and for a selection of the three different Myanmar groups plus sample MYA12

About other trace elements in diopside for Myanmar lapis lazuli, Cr content resulted unusually very low compared to other lapis lazuli provenances (see Fig. 5) and therefore an interesting indicator for a Myanmar origin. Indeed, chromium is for all samples under the limit of detection, with the exception of four crystals: one from sample MYA03 ($9\text{\AA}\pm 3$ ppm) two from sample MYA06 ($9\text{\AA}\pm 2$ and $8\text{\AA}\pm 2$ ppm) and one from MYA07 ($8\text{\AA}\pm 2$ ppm). It must be observed that the average LOD values for Cr are 50 ppm using INFN-LNL set-up and 7 ppm at NewAGLAE. Myanmar samples appear to be also poorer in Mn traces, generally below 150 ppm ; the small cluster visible slightly above 200 ppm is composed only by points related to samples MYA10 and MYA11, i.e. group 2, as can be seen in Fig. 3. Moreover, an element that was not previously included in the operative protocol, but seems to have relevance for Myanmar provenance, is zinc: half of the samples show a Zn content higher than 50 ppm that leads to an incompatibility with an Afghan provenance (Fig. 5). Considering that this feature is not present in all samples, this can only be considered as a weaker marker to distinguish Afghan and Myanmar provenances. Zirconium was found in Myanmar lapis lazuli as well, but the concentrations were not determinant for a discrimination with any other provenance (see Fig. 5). Finally, apart from the copper content (max. $15\pm 5\text{ ppm}$ in sample MYA02), in all the Myanmar samples no other elements occasionally observed in diopside from other provenances were identified, i.e. As (max. LOD = 13 ppm), Pb (max. LOD = 32 ppm), Y (max. LOD = 51 ppm). However, due to the scarce occurrence of these elements in lapis lazuli from other provenances, they cannot be used as marker. Lastly, μ -IBIL spectra acquired for the diopside crystals analysed in this work present the smaller band at 690 nm , similar to the one noticed in some Tajik and Siberian samples [15] but not the band at 770 nm , that can continue to be considered a weaker marker for the Afghan provenance.

Taking into consideration all the results obtained on Myanmar samples, it is possible to include this provenance into the analytical protocol. The flow chart of the protocol could then be modified as suggested in Fig. 7. Strong markers such as wollastonite for Chilean samples and altered pyrites for Siberian samples are confirmed and maintained. The high concentration of strontium in Siberian samples can still be considered a marker, even if a 4% of Myanmar samples showed a Sr content of about 180 ppm that is the lower limit for the Siberian samples; for good measure, this limit is raised to 200 ppm and the marker classified now as weak. The strength of Cu and Ni markers in pyrite is still valid for the distinction between Tajikistan and Afghanistan, but fails in the discrimination from Myanmar samples. No strong markers were found to distinguish between Myanmar and Afghan or Myanmar and Tajik samples, but weaker markers in diopside or pyrite can help in the single differentiations. Specifically, in the Myanmar–Afghanistan uncertainty, only Myanmar samples are characterized by a content of Zn in diopside higher than 50 ppm and only Afghan samples have a Ti content above 800 ppm , a V content above 320 ppm , a Cr content above 75 ppm or a Mn content above 310 ppm (these values were fixed taking into account the maximum values in Table 2 for each elements increased by a standard deviation). Moreover, it was confirmed that the presence of a strong ionoluminescence band centred at about 770 nm [15] is incompatible both with a Tajikistan and Myanmar provenance. As regards the Myanmar–Tajikistan distinction, samples with a Se content in pyrite above 27 ppm (the maximum LOD for Tajik samples) can be assigned to the Myanmar provenance, while those characterized by a Cu content above 180 ppm (as the minimum Cu content measured in Tajik samples is $210\pm 30\text{ ppm}$) and simultaneously a Se content under 26 ppm can be classified as Tajik (see Fig. 6b).

Samples that do not present these markers remain with an uncertain attribution, arising the need to possibly investigate different mineral phases to find new strong markers. This need is enhanced by the limited number of pyrite crystals found in Myanmar samples for IBA (in this study only in 60% of the Myanmar samples suitable pyrite crystals were found). If the analysis is limited only to diopside and not to pyrite crystals, e.g. when the latter is very scarce in the rock sample, to distinguish among Afghanistan

and Tajikistan the elemental contents in diopside found in the previous protocol are still valid, i.e. only Afghan samples show one of the following features: a Ti content above 710 ppm, a V content above 210 ppm or a Cr content above 220 ppm [11, 15].

Lastly, in Fig. 5 for the comparison with other provenances the results from the whole Myanmar sample set were considered. However, it is interesting to observe that when the data from diopside crystals are separated according to the sample grouping previously mentioned, it can be seen an evident discrimination between Afghan samples and single Myanmar groups. As shown in Fig. 8, Zn content can be used for a distinction from group 1 samples, Fe content for group 2 samples or MYA12 and Mn for group 3 samples. For now, these results were not considered for the protocol, due to the possibility that when increasing the statistics on the Mogok area, elemental contents from different mines could overlap.

5 Conclusions

Studies on the provenance of lapis lazuli can greatly improve the knowledge on trade routes active in the ancient past. The importance to have a reference set of samples with certain origin arises when trying to produce an analytical protocol able to attribute a certain provenance to artefacts whose raw material is of unknown origin. Thanks to IBA measurements on new samples acquired in Myanmar, it has been possible to introduce an additional provenance in the analytical protocol developed by our group, currently based on the analysis of diopside, pyrite and wollastonite mineral phases. Features characteristic of the three different Myanmar groups previously identified within the new samples with other techniques were found with IBA, in particular for the different Mn, Fe and Sr concentrations in diopside. From the comparison with other provenances, it was found that Myanmar lapis lazuli is easily distinguishable from Chilean and Siberian rocks thanks to two strong markers, the absence of wollastonite and the well-preserved pyrite crystals, and one weaker marker, the low strontium content in diopside. The combination of Ni and Cu in pyrite remains a strong marker for the differentiation of Afghan and Tajik lapis lazuli. No strong markers were found to distinguish between Myanmar and Afghan or Myanmar and Tajik samples, but weaker markers in diopside or pyrite can help in the single differentiations and in particular the high Zn and the low Ti, V, Cr and Mn concentrations in diopside, the high Se content in pyrite and the absence of the 770 nm band in diopside IBIL spectra. Nevertheless, the need of strong markers is still unsatisfied. For these reasons, the study of different mineral phases by means of IBA techniques is foreseen in the near future.

Acknowledgements The authors wish to warmly thank IPERION CH (Grant Agreement n. 654028) and IPERION HS (Grant Agreement n. 871034) EU Transnational Access programmes for the financial support of SIBILLA project. The EQUIPEX NEW AGLAE research program (n. ANR-10-EQPX-22, French Ministry of Research) is acknowledged. Prof. Luca Martire is greatly acknowledged for the availability of the Cold-CL apparatus.

Funding Open access funding provided by Università degli Studi di Torino within the CRUI-CARE Agreement.

Data Availability Statement All relevant data generated or analysed during this study are included in this manuscript; additional information can be granted upon reasonable request to the authors.

Declarations

Conflict of interest statement The authors have no affiliations with or involvement in any organization or entity with any financial interest or non-financial interest in the subject matter or materials discussed in this manuscript.

Open Access This article is licensed under a Creative Commons Attribution 4.0 International License, which permits use, sharing, adaptation, distribution and reproduction in any medium or format, as long as you give appropriate credit to the original author(s) and the source, provide a link to the Creative Commons licence, and indicate if changes were made. The images or other third party material in this article are included in the article's Creative Commons licence, unless indicated otherwise in a credit line to the material. If material is not included in the article's Creative Commons licence and your intended use is not permitted by statutory regulation or exceeds the permitted use, you will need to obtain permission directly from the copyright holder. To view a copy of this licence, visit <http://creativecommons.org/licenses/by/4.0/>.

References

1. C. Cipriani, C. Innocenti, R. Trosti-Ferroni, *Museol. Sci.* **5**(1–2), 17 (1988)
2. J. Wyart, P. Bariand, J. Filippi, *Gems Gemol.* **17**, 184 (1981)
3. J. Zöldföldi, S. Richter, Z. Kasztovszky, J. Mihaly, in *Proceeding 34th Int. Symp. Archaeom. Zaragoza - Spain 2006*, 353–361 (2004)
4. D.D. Hogarth, W.L. Griffin, *Lithos* **9**, 39 (1976)
5. J.F. Jarrige, in *Forgot. Cities Indus*, ed. by M. Jansen, M. Mulloy, G. Urban (Verlag, Mainz am Rhein, 1991), pp. 34–49
6. A.S. Sofianides, G.E. Harlow, *Gems and crystals from the american museum of natural history* (Simon and Schuster, New York, 1990)
7. I.J. Winter, in *Cornaline Pierres Précieuses La Méditerranée l'Antiquité à l'Islam*, ed. by A. Caubet (Musée du Louvre, Paris, 1999), pp. 43–58
8. M. Mariottini, G. Della Ventura, A. Sodo, M. Vidale, in *Lapis Lazuli bead Mak. Shahr-i Sokhta*, ed. by M. Vidale, A. Lazzari (Ed. Antilia, 2017), pp. 159–199
9. M. Favaro, A. Guastoni, F. Marini, S. Bianchin, A. Gambirasi, *Anal. Bioanal. Chem.* **402**(6), 2195 (2012). <https://doi.org/10.1007/s00216-011-5645-4>

10. B. Keisch, Secrets of the past: nuclear energy application in art and archaeology. Tech. rep., U.S. Atomic Energy Commission (1972)
11. A. Lo Giudice, D. Angelici, A. Re, G. Gariani, A. Borghi, S. Calusi, L. Giuntini, M. Massi, L. Castelli, F. Taccetti, T. Calligaro, C. Pacheco, Q. Lemasson, L. Pichon, B. Moignard, G. Pratesi, M.C. Guidotti, *Archaeol. Anthropol. Sci.* **9**(4), 637 (2017). <https://doi.org/10.1007/s12520-016-0430-0>
12. S. Calusi, E. Colombo, L. Giuntini, A. Lo Giudice, C. Manfredotti, M. Massi, G. Pratesi, E. Vittone, *Nucl. Instruments Methods Phys. Res. Sect. B Beam Interact. with Mater. Atoms* **266**(10), 2306 (2008). <https://doi.org/10.1016/j.nimb.2008.03.077>
13. C. Czelusniak, L. Palla, M. Massi, L. Carraresi, L. Giuntini, A. Re, A. Lo Giudice, G. Pratesi, A. Mazzinghi, C. Ruberto, L. Castelli, M. Fedi, L. Liccioli, A. Gueli, P.A. Mandò, F. Taccetti, *Nucl. Instruments Methods Phys. Res. Sect. B Beam Interact. with Mater. Atoms* **371**, 336 (2016). <https://doi.org/10.1016/j.nimb.2015.10.053>
14. A. Lo Giudice, A. Re, S. Calusi, L. Giuntini, M. Massi, P. Olivero, G. Pratesi, M. Albonico, E. Conz, *Anal. Bioanal. Chem.* **395**(7), 2211 (2009). <https://doi.org/10.1007/s00216-009-3039-7>
15. A. Re, D. Angelici, A. Lo Giudice, J. Corsi, S. Allegretti, A.F. Biondi, G. Gariani, S. Calusi, N. Gelli, L. Giuntini, M. Massi, F. Taccetti, L. La Torre, V. Rigato, G. Pratesi, *Nucl. Instruments Methods Phys. Res. Sect. B Beam Interact. with Mater. Atoms* **348**, 278 (2015). <https://doi.org/10.1016/j.nimb.2014.11.060>
16. D. Angelici, A. Borghi, F. Chiarelli, R. Cossio, G. Gariani, A. Lo Giudice, A. Re, G. Pratesi, G. Vaggelli, *Microsc. Microanal.* **21**(2), 526 (2015). <https://doi.org/10.1017/S143192761500015X>
17. A. Re, D. Angelici, A. Lo Giudice, E. Maupas, L. Giuntini, S. Calusi, N. Gelli, M. Massi, A. Borghi, L.M. Gallo, G. Pratesi, P.A. Mandò, *Appl. Phys. A Mater. Sci. Process.* **111**(1), 69 (2013). <https://doi.org/10.1007/s00339-013-7597-3>
18. G. Vaggelli, L. Es Sebar, A. Borghi, R. Cossio, A. Re, F. Fantino, A. Lo Giudice, *Eur. Phys. J. Plus* **134**(3) (2019). <https://doi.org/10.1140/epjp/i2019-12523-4>
19. T. Themelis, *Gems and Mines of Mogok* (A &T Pub, USA, 2008)
20. L. Guidorzi, A. Re, F. Picollo, P. Aprà, F. Fantino, L. Martire, G. Artioli, L. Peruzzo, S. Boesso, V. Rigato, L. La Torre, A. Lo Giudice, *Nucl. Inst. Methods Phys. Res. B* **479**, 143 (2020). <https://doi.org/10.1016/j.nimb.2020.06.035>
21. J. Forneris, A. Lo Giudice, P. Olivero, F. Picollo, A. Re, M. Marinelli, F. Pompili, C. Verona, G. Verona Rinati, M. Benetti, D. Cannata, F. Di Pietrantonio, *Europhys. Lett.* **108**(1) (2014). <https://doi.org/10.1209/0295-5075/108/18001>
22. A. Battiato, M. Lorusso, E. Bernardi, F. Picollo, F. Bosia, D. Ugues, A. Zelferino, A. Damin, J. Baima, N.M. Pugno, E.P. Ambrosio, P. Olivero, *Acta Mater.* **116**, 95 (2016). <https://doi.org/10.1016/j.actamat.2016.06.019>
23. F. Picollo, A. Battiato, E. Bernardi, M. Plaitano, C. Franchino, S. Gosso, A. Pasquarelli, E. Carbone, P. Olivero, V. Carabelli, *Sci. Rep.* **6**, 1 (2016). <https://doi.org/10.1038/srep20682>
24. S. Gama, M. Volfinger, C. Ramboz, O. Rouer, *Nucl. Inst. Methods Phys. Res. B* **181**, 150 (2001). [https://doi.org/10.1016/S0168-583X\(01\)00350-0](https://doi.org/10.1016/S0168-583X(01)00350-0)
25. J.L. Campbell, N.I. Boyd, N. Grassi, P. Bonnick, J.A. Maxwell, *Nucl. Instruments Methods Phys. Res. Sect. B Beam Interact. with Mater. Atoms* **268**(20), 3356 (2010). <https://doi.org/10.1016/j.nimb.2010.07.012>
26. L. Giuntini, L. Castelli, M. Massi, M. Fedi, C. Czelusniak, N. Gelli, L. Liccioli, F. Giambi, C. Ruberto, A. Mazzinghi, S. Barone, F. Marchegiani, S. Nisi, C. Lubritto, S. Altieri, L. Tortora, P. Branchini, A. Fabbri, V. Graziani, S. Barcellos Lins, L. Guidorzi, A. Lo Giudice, A. Re, L. Sottili, A. Balerna, M. Cestelli Guidi, S. Altieri, M. Bonesini, D. Di Martino, M. Clemenza, M. Carpinelli, P. Oliva, V. Sipala, A.M. Gueli, S. Pasquale, G. Stella, G. Pepponi, F. Grazi, F. Taccetti, *Appl. Sci.* **11**(3462) (2021). <https://doi.org/10.3390/app11083462>
27. L. Pichon, B. Moignard, Q. Lemasson, C. Pacheco, P. Walter, *Nucl. Instruments Methods Phys. Res. Sect. B Beam Interact. with Mater. Atoms* **318**(PART A), 27 (2014). <https://doi.org/10.1016/j.nimb.2013.06.065>
28. L. Pichon, T. Calligaro, V. Gonzalez, Q. Lemasson, B. Moignard, C. Pacheco, *Nucl. Instruments Methods Phys. Res. B* **348**, 68 (2015). <https://doi.org/10.1016/j.nimb.2015.01.010>
29. L. Pichon, T. Calligaro, Q. Lemasson, B. Moignard, C. Pacheco, *Nucl. Instruments Methods Phys. Res. Sect. B Beam Interact. with Mater. Atoms* **363**, 48 (2015). <https://doi.org/10.1016/j.nimb.2015.08.086>
30. M. Gaft, R. Reisfeld, G. Panczer, *Modern luminescence spectroscopy of minerals and materials* (Springer Mineralogy, 2015)